Alignment and instability of dust crystals in plasmas

V. A. Schweigert,[1] I. V. Schweigert,[2] A. Melzer,[3] A. Homann,[3] and A. Piel[3]

[1]*Insitute of Theoretical and Applied Mechanics, Novosibirsk, 630090, Russia*
[2]*Institute of Semiconductor Physics, Novosibirsk, 630090, Russia*
[3]*Institut für Experimentalphysik, Christian-Albrechts-Universität Kiel, 24098 Kiel, Germany*

Charged dust particulates, forming a layered crystal in the electrode sheath of a rf discharge, are known to show vertical alignment and an onset of characteristic oscillations below a threshold of neutral gas density. Here forces on the particulates due to the formation of positive space-charge clouds below the dust particles are calculated from Monte Carlo calculations of the ion motion in the sheath. The forces are shown to be attractive and nonreciprocal for the different crystal layers. From the Monte Carlo results an analytical lattice model is derived that quantitatively explains the experimental findings. [S1063-651X(96)06710-4]

I. INTRODUCTION

Wigner crystallization of micrometer ''dust'' particles has attracted much interest in the field of plasma physics recently. The dust particles acquire high negative charges like floating probes and interact by means of their Coulomb repulsion. If the Coulomb energy of neighboring particles by far exceeds their thermal energy, the particles arrange in ordered solidlike structures. The existence of these so-called plasma or dust crystals was predicted by Ikezi [1]. Experimentally they were found in magnetron rf discharges [2–4] and in parallel plate rf discharges [5–7]. The dust crystal is trapped in the sheath of the lower electrode where the electric field force on the particles balances the force of gravity. The particles usually form a flat crystal of about 100×100 elementary cells width, but of only a few layers thickness. In the horizontal plane, these crystals show hexagonal order as usually found in two-dimensional (2D) systems, but in the vertical direction the particles are aligned rather than being arranged in close-packed structures [4,7]. Close-packed structures are expected for 3D crystals as well as for laterally infinite crystals having two or more layers embedded in a uniform positive background [8,9]. For screened potentials this aligned structure cannot be established as well [10].

Another peculiarity of the plasma crystal is observed when the density of the filling gas is reduced. Then the dust particles acquire high random kinetic energies (i.e. high temperatures) below a certain pressure threshold [11,12]. Due to this increase in dust temperature the plasma crystal performs a phase transition from the solidlike structure to a liquid state. At this phase boundary self-excited oscillations of the particles in the plasma crystal appear. These oscillations are interpreted in Refs. [11,13] as a precursor of the temperature increase, in the sense that the oscillations originate from a plasma instability and grow more and more violent finally leading to the strong erratic dust particle motion. In Ref. [12], however, the oscillations are attributed to the mixed two- and three-dimensional nature of the crystal or as a new intermediate state of the melting transition. It is known [11] that the described phase transition is observable for plasma crystals of two or more layers only. So we restrict further discussion to the case of a two-layer crystal, for simplicity.

The observed oscillations have the following features [13]. Vertical pairs of particles oscillate horizontally about their aligned equilibrium position at a frequency of about 13 Hz. The oscillation amplitude of the lower particle is about twice that of the upper one and the upper particle has a phase lead of about $45° \pm 30°$. These oscillations suddenly appear below a certain pressure threshold. At this pressure all externally forced oscillations are damped within milliseconds.

To understand this unexpected behavior of alignment and oscillations of the plasma crystal one has to investigate the interparticle forces in the sheath of a rf discharge. Particles of radius R attain a charge $Ze = R U_f$ in the plasma environment (cgs units are used here), where U_f is the floating potential of the particle. The measured charges are $Z \simeq 10^4$ for $R = 4.7$ μm particles [6,7,11].

''Drag'' forces on such particles due to external fields and screening of the particles have been studied in several investigations [14–17]. The interparticle potential in a quasineutral plasma can be described by a Debye-Hückel law [18]. However, these forces cannot be applied to the problem of alignment and oscillations because in the sheath, where the dust crystal is located, the plasma is strongly non-neutral. Furthermore, one has to know not only the forces due to external fields, but also interparticle forces arising from deviations from the equilibrium particle position in direction of the external field and perpendicular to it.

The formation of space-charge regions below the dust particles by ion focusing in the sheath as a possible explanation of the alignment was also put forth by Melandsø and Goree [19] and by Vladimirov and Nambu [20]. But their collisionless models have only limited applicability in the region of pressures considered here and resulting forces on the particles were not calculated from such models.

So an explanation of the mechanism of the unstable oscillations as well as a convincing proof that the vertical alignment is energetically more favorable than close-packed structures are still lacking. For this reason, we will present here Monte Carlo (MC) calculations of the ion streaming motion in the sheath in the presence of a two-layer dust crystal for conditions found in our experiments. The formation of ion space-charge clouds on the downstream side of the particles is found to persist even under the collisional
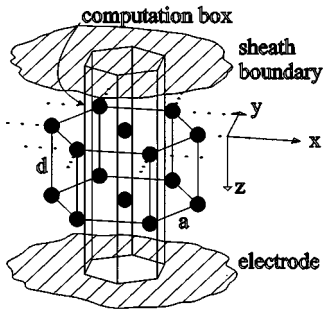
FIG. 1. Sketch of the modeled system.

conditions. Forces on the particles are calculated from the ion trajectories. Based on these MC results an analytical crystal model introducing an additional crystal layer of positive ''cloud'' charges is presented. This model is used to study quantitatively the vertical alignment and the oscillation characteristics as a consequence of a plasma-induced instability. A simplified 1D version of this model was discussed in [13].

The Monte Carlo model is presented in Sec. II and the results are discussed in Sec. III. The analytical crystal model is derived in Sec. IV. The unstable oscillations are discussed in Sec. V and compared with the experiment. Conclusions are presented in Sec. VI.

II. MONTE CARLO MODEL FOR THE ION MOTION CALCULATION

The system of a two-layer plasma crystal with hexagonal order in the horizontal plane and vertically aligned particles in the sheath of an rf discharge is considered (see Fig. 1). To give numbers we adopt the experimental values of Melzer *et al.* [11,13]. The results of our calculations can also easily be applied to other experiments [5,12] because the experimental conditions are similar.

In these experiments a rf discharge is operated in helium at a pressure of $p = 30$–150 Pa and a power input of 12 W. The plasma crystal is formed by spherical, monodisperse particles of $R = 4.7$ μm radius and mass $M = 6.73 \times 10^{-13}$ kg with a negative potential of $-U_f = 2$–5 V corresponding to $Z = 6000$–15 000 elementary charges. For the MC calculations a potential of -5 V is used unless stated otherwise. The interparticle distance in the horizontal plane is $a = 450$ μm and in the vertical direction $d = 360$ μm $= 0.8a$. The frictional damping ν exerted by the neutral gas background on the dust grains is $\nu \simeq 12$ s^{-1} at 30 Pa [21].

We restrict our approach here to a non-self-consistent description of our problem in three dimensions, which means that ion-ion interactions are neglected and the charge on the particles is fixed rather than being determined from the electron and ion flux onto it. A self-consistent approach is beyond our present computational power, but the experimental results for the parameters of a layered crystal such as the particulate charge, interparticulate distance, and interlayer spacing permit us to simplify our model description.

The ion flux entering through the plasma-sheath boundary is assumed to be horizontally uniform. The ions are accelerated in the sheath by a strong electric field. Due to collisions

some ions can be trapped in the potential well of the charged particulates. The others finally reach the electrode surface. Resonant charge exchange determines the ion mean free path. At the pressure of interest the ion mean free path λ_{mfp} is within a range of 50–200 μm. Usually $\lambda_{mfp} = 100$ μm, corresponding to a pressure of 100 Pa, is used for simulation.

In the transverse (horizontal) plane (x,y) the charged grains are arranged in an infinite hexagonal lattice with the translation vectors $\vec{\rho} = n_1 \vec{a}_1 + n_2 \vec{a}_2$, where n_1 and n_2 are any integers and $\vec{a}_1 = (a,0)$ and $\vec{a}_2 = (a/2, \sqrt{3}a/2)$ are the primitive translation vectors of the Bravais lattice. The vertical (longitudinal) direction is denoted with z (see Fig. 1).

The total potential of the crystal-plasma system is the sum of the sheath potential and that of the two hexagonal layers of charged particles. It is convenient to represent the potential of a lattice layer of negative point charges φ as $\varphi(\vec{r}) = \varphi_0(z) + \varphi_1(\vec{r})$. The potential $\varphi_1(\vec{r})$ describes the negative point charges embedded in a horizontally uniform sheet of compensating positive charges, described by a Dirac δ function in the vertical direction. The effect of the positive sheet is neutralized by $\varphi_0(z)$, where $\varphi_0(z) = \int \varphi(\vec{\rho},z)d\vec{\rho}$. The integration is performed over the transverse coordinates $\vec{\rho} = (x,y)$, thus $\varphi_0(z)$ is independent of the transverse coordinates.

Using the Fourier transform over the translation vectors of the lattice, $\varphi_1(\vec{r})$ can be written as the sum over the translation vectors $\vec{g}$ of the reciprocal lattice

$$\varphi_1(\vec{\rho},z) = -\sum_{g,g \neq 0} \frac{4\pi e Z}{gS} \exp(-g|z|)\exp(i\vec{g}\cdot\vec{\rho}), \quad (1)$$

$$\vec{g} = n_1 \vec{b}_1 + n_2 \vec{b}_2, \quad g = |\vec{g}|,$$

where $\vec{b}_1 = (2\pi/a, -2\pi/\sqrt{3}a)$ and $\vec{b}_2 = (0, 4\pi/\sqrt{3}a)$ are the primitive reciprocal translation vectors and $S = \sqrt{3}a^2/2$ is the area of an elementary cell. It is seen from Eq. (1) that for large distances z from a layer the potential depending on transverse coordinates falls off exponentially with increasing z. This means that an ion does not ''feel'' the pointlike structure of the lattice at distances from the lattice greater than a certain value $z_\star$. This characteristic length $z_\star$ is determined by the minimal value of the reciprocal lattice vector $g_{min} \approx 2\pi/a = 1/z_\star$. For our experimental conditions $z_\star \approx 70$ μm. This length is much shorter than the distance from a layer to both the electrode and the quasineutral bulk plasma. Therefore, one can neglect the influence of image charges in the metallic electrode and the plasma. To calculate φ_1 numerically according to Eq. (1) the Ewald technique [22] is applied.

The plasma crystal is suspended in the sheath by an upward directed electric-field force ZeE, which is balanced by the gravitational force Mg. The longitudinal electric field E is created by the two uniform crystal layers with a vertical distance d as well as the ion and electron volume charge in the plasma sheath. We use a common sheath model [23] where the time-averaged volume charge density ϱ is as-

sumed to be constant and independent of horizontal coordinates. Solving Poisson's equation for the time-averaged longitudinal electric field E

$$\frac{\partial E}{\partial z} = 4\pi[\varrho - \varrho_l \delta(z-z_1) - \varrho_l \delta(z-z_2)], \qquad (2)$$

with condition $E(z=0)=0$ on the plasma-sheath boundary, the longitudinal field in the sheath is

$$E(z) = \begin{cases} 4\pi\varrho z, & 0<z<z_1 \\ 4\pi(\varrho z-\varrho_l), & z_1<z<z_2 \\ 4\pi(\varrho z-2\varrho_l), & z>z_2, \end{cases} \qquad (3)$$

where $\varrho_l = eZ/S$ is the negative 2D charge density of the crystal layers and z_1 and z_2 are the distances from the plasma-sheath boundary to the upper and lower layer, respectively. ϱ, z_1, z_2 are obtained from the condition of equilibrium between gravity and the electric force for both layers and $z_2 - z_1 = d$ with the experimentally given interlayer distance d. The distance between the upper layer and the plasma sheath boundary is then $z_1 = d(1/2 + gM/4\pi eZ\varrho_l)$, and this condition allows, in principle, one to find the particulate charge by measuring the position of the upper layer relative to the plasma-sheath boundary [6]. The volume charge density is found as $\varrho = eZ/dS$, which means that the interlayer repulsion is completely compensated by the attraction of the positive background contained between the two crystal layers. For a particulate floating potential $U_f = -5$ V the electric field $E_0 = Mg/Z$ at the particulate location is about 25 V/cm and the volume charge density is $\varrho = 2.6 \times 10^8$ cm^{-3}, which is in agreement with measured values [6,7].

Two kinds of forces acting on a particle due to the particle-ion interaction are considered. First, ions hitting the (completely absorbing) particulate transfer their momentum to the particle, resulting in a force

$$\vec{F}_1 = \int m_i \vec{v}_i n_i (\vec{v}_i \cdot d\vec{\sigma}), \qquad (4)$$

where $m_i, \vec{v}_i, n_i$ are the mass, the velocity, and the density of ions, respectively, and $d\vec{\sigma}$ is an orientated surface element of the particle.

Second, the Coulomb interaction between ions and a particulate gives the contribution

$$\vec{F}_2^k = \int e n_i(\vec{r}) \vec{\nabla} \varphi_1(\vec{\rho}, z-z_k) d\vec{r}, \quad k=1,2. \qquad (5)$$

The integration extends over the area of an elementary hexagonal cell. Note that the potential φ_1 includes the ions in the considered elementary cell as well as all periodic images.

The upper boundary of calculation region $z=0$ is set sufficiently far upstream of the crystal. The ion density at the upper boundary is fixed to a specific value $n_t \gtrsim \varrho$. All forces discussed below are proportional to this parameter n_t. The lower boundary of the computation region represents a completely absorbing electrode. Horizontally, the computation region is chosen as an elementary cell of the hexagonal lattice with periodic boundary conditions. In the computation cell, finally there is one particulate for each layer. Ion
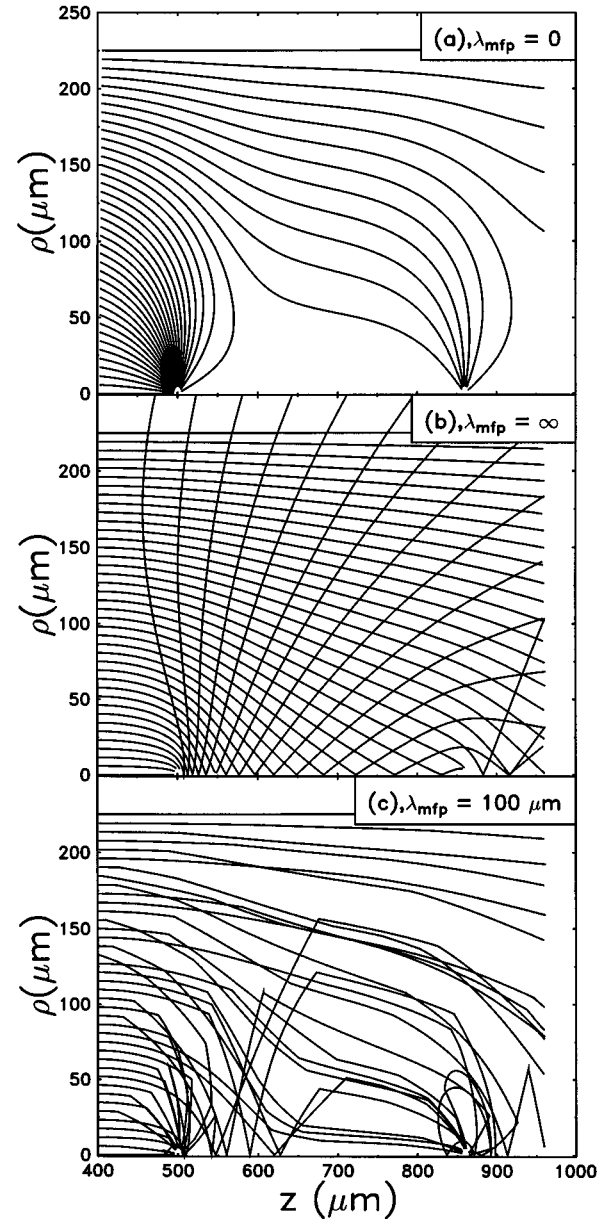
FIG. 2. Ion trajectories (a) in a pure drift regime, (b) in a pure collisionless regime, and (c) for a collisional case with ion mean free path $\lambda_{mfp} = 100$ μm due to ion charge-exchange collisions, which are indicated by kinks in the trajectories. The particle positions are $z=500$ μm (upper) and $z=860$ μm (lower).

charge-exchange collisions are taken into account. Statistic errors of the calculation are given in some of the figures.

III. RESULTS OF MONTE CARLO CALCULATIONS

To understand the resulting ion distribution, first two limiting cases of the ion motion are considered: (a) the drift regime ($\lambda_{mfp} \rightarrow 0$) and (b) the collisionless case ($\lambda_{mfp} \rightarrow \infty$). Due to the attraction of the ions by the particles the ions are deflected. For the drift regime ion trajectories mainly terminate *on* the upper particulates. Immediately behind them shadowed areas of low ion density appear [Fig. 2(a)]. These rarefaction areas extend to the lower particles. The opposite behavior is found in the collisionless limit [Fig. 2(b)]. Re-
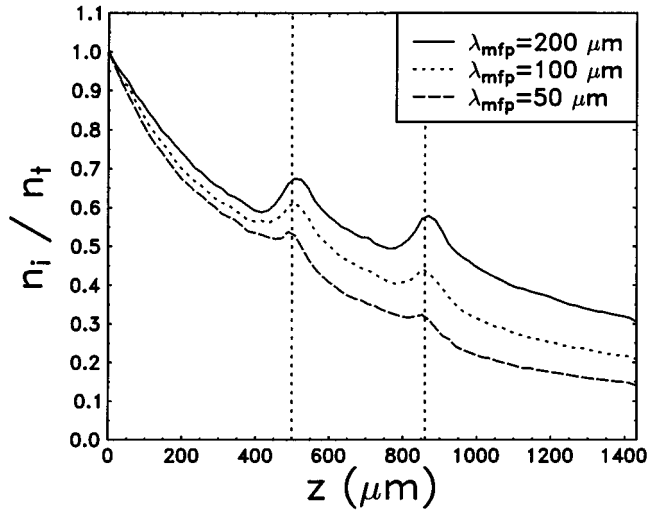
FIG. 3. Ion density distribution averaged over the (x,y) plane for different ion mean free paths. The vertical dashed lines indicate the particle positions at $z = 500$ μm and $z = 860$ μm.

gions of enhanced ion density occur below the upper particles and extend over a wide range of z. The kinetic energy of the ions is so high that the ions are not captured by the particles. This leads to ion focusing *below* the particles. The gas pressure range of 50–200 Pa is an intermediate case ($\lambda_{mfp} = 50$–200 μm is smaller but of the order of d), where the ion velocity is not a local function of the electric field. A small sample of ion trajectories obtained by Monte Carlo technique for this case are given in Fig. 2(c).

The calculated ion density distributions for aligned particles are given in Figs. 3 and 4. Figure 3 shows the ion density averaged over transverse coordinates (x,y) as a function of the vertical position. In general, the density decreases towards the electrode since the ions are accelerated in the sheath. The maxima in ion density are associated with the positions of the particles in the upper ($z_1 = 500$ μm) and lower layer ($z_2 = 860$ μm). It is seen that with increasing pressure (reduced λ_{mfp}) the ion focusing effect is diminished. The maxima in ion density are not very large because the density is averaged over the transverse plane and the regions of enhanced ion density are localized, as can be seen in Fig. 4. There contour plots of the ion density in the (ρ,z) plane (averaged over azimuthal angle) for $\lambda_{mfp} = 100$ μm are shown. One can identify three different regions. In the closest vicinity of the particulates (region I) the ion density is strongly enhanced (by a factor of 10) due to trapping of ions in the potential well of the particles. The size of the potential well L in the direction of ion flow can be estimated by equating the Coulomb field of the particles and sheath electric field at the particles position. $L = \sqrt{eZ/E_0} < 100$ μm for our conditions. As pointed out above, the transverse component of the field of a layer quickly decays with distance. Therefore, if an ion is outside the potential well, i.e., $|z - z_1| \gtrsim L \sim z_\star$, ion-neutral collisions weakly deflect an ion in the transverse direction.

Below the particulates, a region of enhanced ion density (ion cloud) is formed by focused ions (region II). There the ion density attains a few times its unperturbed value. The formation of this ion cloud is one of the crucial findings of
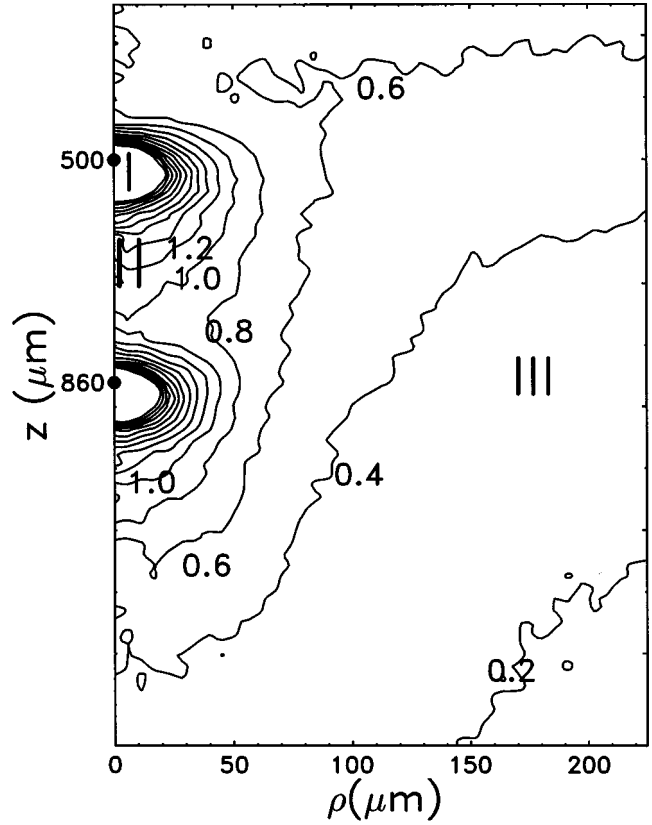
FIG. 4. Ion density distribution in cylindrical coordinates averaged over azimuthal angle in the case of alignment for $\lambda_{mfp} = 100$ μm. The numbers give the ion density in units of n_t.

the MC calculations. It has been shown here that the ion focus region found in collisionless systems [19,20] is also preserved under the more realistic conditions considering collisions and the presence of a lower particle layer. This ion-cloud region provides attractive forces for the negatively charged particles. In region III the ion density in radial direction changes weakly. The ions almost do not feel the presence of the particulates. There one finds only the usual reduction of ion density in the longitudinal direction due to ion acceleration in the sheath.

In the layered structure with vertical alignment there is no "net" horizontal force acting on particulates due to the hexagonal symmetry in the horizontal direction, but small deviations from the aligned positions will induce horizontal repulsive (due to particle-particle interaction) and attractive forces (due to particle–ion-cloud interaction) on the particles. In order to study the stability of this arrangement calculations of the ion distribution and the resulting forces for different displacements of the lower-layer lattice relative to the upper layer are performed. From the above-mentioned estimates one can expect that the lower layer is able to influence ion trajectories only for $|z - z_2| < z_\star$. This is substantiated in Fig. 5, where the regions of maximum ion density are plotted for various interlayer planes. Here the lower particulates are shifted by $0.25a$ in the x direction from their "aligned" equilibrium positions. The contour lines comprise the regions where the ion density is more than 90% of the maximum ion density for that interlayer plane. One can see that even though the lower particulates are shifted, the ion clouds
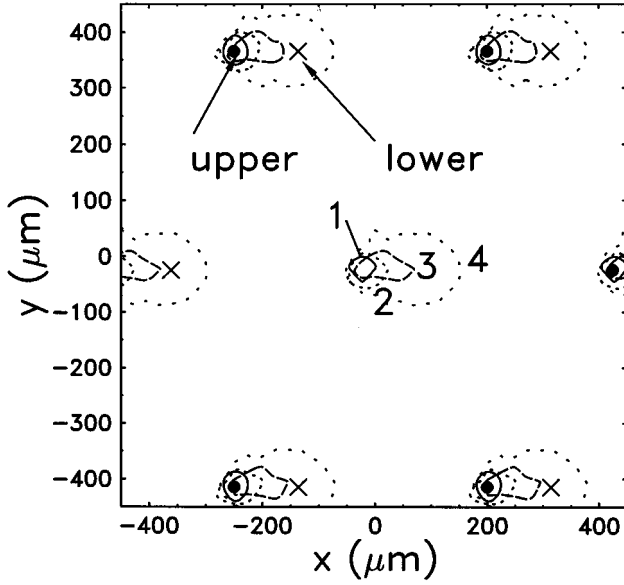
FIG. 5. Shifting of the ion cloud in the (x,y) plane for different z. The displacement of lower particulates from the aligned position is $0.25a$. The contour lines comprise the region of highest ion density in each plane: (1) plane of the upper layer $z=z_1$, (2) $z=0.4d$ above the lower layer plane, (3) $z = 0.2d$ above the lower layer plane, and (4) plane of the lower layer $z=z_2$. Dots and crosses indicate the upper and lower particle positions, respectively.

FIG. 6. Transverse restoring forces from the ion clouds acting on the lower particulates as a function of the displacement in the x direction for different ion mean free paths. (1) $\lambda_{mfp}=50$ μm, $Z_i=0.58Zn_i/\rho$, $d_i=0.49a$; (2) $\lambda_{mfp}=100$ μm, $Z_i=0.43Zn_i/\rho$, $d_i=0.40a$; (3) $\lambda_{mfp}=200$ μm, $Z_i=0.44Zn_i/\rho$, $d_i=0.38a$. Symbols denote the MC results, solid lines indicate the forces for positive point charges with parameters Z_i,d_i replacing the ion cloud. (4) The dashed line is the repulsion force between two layers for $n_t=\varrho$.

remain located directly below the upper particulates. Only very close to the lower particle layer (curve 3) a displacement of the ion cloud becomes observable. Hence the ion cloud depends only on the obstacle on the upstream side, but stays nearly unaffected by the structure on the downstream side. The fact that the ion cloud is found to be coupled with the upper particle is the second main finding of the MC calculations.

The resulting transverse forces on the particles of the lower layer calculated from the MC model are shown in Fig. 6 as a function of the displacement from the aligned positions in the x direction. The most interesting result is the appearance of negative, i.e., restoring forces (curves 1–3, symbols). These forces arise from the attraction of the lower particles by the ion clouds. The force becomes zero at displacements $\delta x=0,a/2$, as expected from symmetry. Any perturbation of these equilibrium positions leads to a restoring of the system to the aligned structure with $\delta x=0$. The forces reach their maximum at $\delta x=0.2a-0.25a$ depending on the ion mean free path λ_{mfp}. A pressure reduction leads to a stronger restoring force. For comparison, the pure Coulomb repulsion force between the layers is included (curve 4). One can see that the restoring force by the ion-cloud attraction decisively exceeds the dust particle Coulomb repulsion. Therefore the aligned structure of the crystal observed in the experiment is favored over the hcp crystal structure. It is important to note that such transverse attractive forces by the ion clouds do not exist for the particles of the upper layer since the ion cloud is located below the upper particle.

For further analytical analysis each ion cloud is replaced by a positive point charge of charge Z_i located below the upper particle at a distance $d-d_i$. Since the position of the ion cloud only weakly depends on the lower-layer position,

as seen above, the positive point charge is treated as rigidly connected to the upper particle. The values of Z_i and d_i are chosen in such a way that the restoring forces due to the positive point charges mimic the restoring forces found from the MC calculations for the different values of the displacement δx within the errors of the MC results (see Fig. 6, solid lines). In the range of pressures set by the experiment, for the effective charge Z_i values of $0.3-0.6$ Zn_t/ϱ, and for the distance d_i values of $0.4-0.6$ a are obtained (see Table I). For characteristic values $n_t/\varrho = 1-3$ the effective positive charge matches the charge of the particulates within an order of magnitude. However, for the lower particulates the attraction by the ion cloud exceeds the repulsion with upper particulates since $d_i<d$. The replacement of the ion cloud by positive point charges for a "static" displacement of the lower-layer particles is justified since the ion relaxation time is much shorter than the period of dust oscillations. Of course, ion-ion interaction that is not taken into account in the MC model above will diminish the effective charge of

TABLE I. MC results for Z_i,d_i for various simulation parameters.

λ_{mfp} (μm)	$-U$ (eV)	d (μm)	$Z_i/Zn_t\varrho^{-1}$	d_i/a	d_i/d
50	5	360	0.58	0.49	0.61
100	5	360	0.43	0.40	0.50
100	5	450	0.42	0.43	0.53
100	3	360	0.25	0.35	0.44
200	5	360	0.44	0.38	0.47

the ion cloud. But since the particle-particle repulsion is considerably less than the particle–ion-cloud attraction it is reasonable to assume that the qualitative picture described above does not change after considering ion-ion interactions. Since the radial component of the lattice electric field decreases exponentially with distance, the restoring force may exist even in the case when the effective ion-cloud charge is much less than that of the particulates.

The main results of the MC simulations are summarized here to enlighten the derivation of the analytical model. Below the particles of the upper layer a positive space-charge region is formed, which results in attractive forces for the lower particles. This ion cloud can be replaced to a good approximation by a single positive point charge of charge Z_i and distance d_i above the lower layer. The ion cloud is found to be located almost directly below the upper particle independent of the position of the lower particles. Therefore the positive point charge can be treated as rigidly connected to the upper particle. Furthermore, due to the fact that the ion cloud is located below the upper particle no attractive forces on the upper particles exist. These points found as results from the MC calculations are the main ingredients of our analytical model.

IV. ANALYTICAL CRYSTAL MODEL

A model is presented here that allows us to describe the dust crystal structure and stability analytically. The crystal instability leading to the heating of the dust particles is treated in a linear stability analysis. In the linear approximation the motion of the particulates in the longitudinal (z) and transverse (x,y) directions is decoupled, since for longitudinal displacements the transverse forces acting on the particulates remain zero due to the symmetry of the system. This is confirmed by experimental observations [11,13], which show that the amplitudes of the transverse particulate oscillations are much larger than those of the longitudinal motion. Therefore, we can restrict the analysis of the particle motion to the plane $\vec{\rho}_{ik} = (x_{ik}, y_{ik})$ at fixed longitudinal coordinate z, where the index i denotes the number of a particulate in a crystal layer and $k = 1,2$ denotes the upper ($k=1$) and lower layer ($k=2$). To calculate the particulate motion the particle-particle interaction and the influence of ions and neutral gas are taken into account. We consider the particle-particle interaction and particle-ion interaction explicitly. The particle-ion interaction is approximated by the particle–positive-point-charge interaction discussed above. The influence of electrons in the sheath can be accounted for as an isotropic screening. Forces from the particulate–neutral-gas collisions are not treated as random in our model, therefore the kinetic energy of particulates is zero in the equilibrium state, but these collisions are considered as velocity-dependent friction forces [21].

Then the Newton equations for our system can be written as

$$\frac{d^2\vec{\rho}_{ik}}{dt^2} = \frac{\vec{F}_{ik}}{M} - \nu\frac{d\vec{\rho}_{ik}}{dt}, \tag{6}$$

where ν is the friction constant and M is the particulate mass. The forces $\vec{F}_{ik} = \vec{F}_{ik,pp} + \vec{F}_{ik,pi}$ acting on the particu-

lates are due to particulate-particulate $\vec{F}_{ik,pp}$ and particulate-ion $\vec{F}_{ik,pi}$ interaction. The particulate-particulate forces can be written as usual as $\vec{F}_{ik,pp} = -\partial U_{pp}/\partial\vec{\rho}_{ik}$, where

$$U_{pp} = \sum_{i>j}\sum_{k=1}^{2} U(|\vec{\rho}_{ik} - \vec{\rho}_{jk}|) + \sum_{i,j} U(|\vec{\rho}_{i1} - \vec{\rho}_{j2} + \vec{e}_z d|) \tag{7}$$

is the total potential of particulate-particulate interaction and $\vec{e}_z$ is the unit vector in longitudinal direction. The first term describes the interaction of particles in the same layer and the second gives the interaction between particles in the upper and lower layers. The interparticle potential U considered here is a pure Coulomb potential $U(r) = e^2 Z^2/r$ only. Debye-Hückel potentials can be used to account for electron screening. But since the electron screening length under the experimental conditions is of the order of $1a-4a$ the difference between Coulomb and Debye-Hückel potentials is small. Screening by ions leads in a first approximation only to a renormalization of the dust particle charge [24].

It was found from the Monte Carlo results that the particle-ion interaction is negligible for the upper particle since the ion cloud is located directly below the upper particle. For the lower particle the interaction with the ions is approximated by the interaction with a positive point charge. Therefore, the particulate-ion forces can be written as $\vec{F}_{ik,pi} = -\delta_{k2}\partial U_{pi}/\partial\vec{\rho}_{ik}$, where U_{pi} is the potential of the positive point charges replacing the ion clouds below the upper particulates. The Kronecker δ_{ik} provides that the attraction is acting on the lower particles only. Then we can describe both the ion-particulate and particulate-particulate interactions by effective pair potentials. This is the main assumption of our model. By this means, the potential of the ion cloud can be written as

$$U_{pi} = -\epsilon\sum_{i,j} U(|\vec{\rho}_{i1} - \vec{\rho}_{j2} + \vec{e}_z d_i|), \quad \epsilon = Z_i/Z. \tag{8}$$

The potential is that of a positive point charge Z_i situated at a distance $d-d_i$ below the upper particulate as found from the MC results. Note the differences between U_{pi} and the second term in U_{pp} decribing the interaction of the lower-layer particles with the point charges and with the particles of the upper layer, respectively. U_{pi} is negative (attractive) and is evaluated at a vertical distance d_i rather than d, but the positions ρ_{i1} are the same for the upper particle and for the positive point charge since they are treated as rigidly connected.

The total force on the particles is then

$$\vec{F}_{ik} = -\frac{\partial U_{pp}}{\partial\vec{\rho}_{ik}} - \delta_{k2}\frac{\partial U_{pi}}{\partial\vec{\rho}_{ik}}. \tag{9}$$

Note that for the forces given by the Eq. (9) Newton's third law *actio = reactio* is not valid. This is because of the ions that give the essential contribution to the forces acquire their momentum in the external electric field and lose it in the collisions with gas atoms. The symmetry breaking by the ions streaming from above through the crystal leads to the nonreciprocity of the forces. This situation is typical for *open*

system, which cannot be described by any Hamiltonian. The breaking of Newton's *actio=reactio* law is the main reason for the heating mechanism of the particles. In contrast, all Hamiltonian systems without friction conserve their total energy. Hamiltonian systems with friction achieve a metastable state with zero kinetic energy.

V. CRYSTAL INSTABILITY

A. General results

Now a linear stability analysis of the system described by Eqs. (6) and (9) is performed. Therefore small deviations $\xi_{\alpha i,k}=\zeta_{\alpha k}(\vec{q})\exp(\lambda t+i\vec{q}\cdot\vec{\rho}_{ik})$ from the vertical aligned positions ρ_{ik} are considered, where $\vec{q}$ is the spatial wave vector of the displacement. $x_{\alpha},\alpha=1,2$, indicates the directions x,y. Substituting this into Eq. (6), we find the values of $\zeta_{\alpha k}$ as the eigenvectors of the dynamical matrix

$$A_{\alpha k,\beta n}=-\frac{1}{M}\sum_{\vec{\rho}_j=\vec{\rho}_i+\vec{\rho}}\left(\frac{\partial^2 U_{pp}}{\partial x_{\alpha i,k}\partial x_{\beta j,n}}\right.$$
$$\left.+\delta_{k2}\frac{\partial^2 U_{pi}}{\partial x_{\alpha i,k}\partial x_{\beta j,n}}\right)e^{i\vec{q}\cdot(\vec{\rho}_j-\vec{\rho}_i)}, \quad (10)$$

where the summation is performed over all translation vectors $\vec{\rho}$ of the hexagonal lattice. Since the dynamical matrix (10) is expressed through the lattice sums, a numerical technique is necessary to obtain its eigenvalues. An expanded form of the dynamical matrix can be written as

$$A=\begin{pmatrix} -W_{\alpha\beta}+S_{\alpha\beta}(0) & -S_{\alpha\beta}(\vec{q}) \\ -S_{\alpha\beta}(\vec{q})+\epsilon D_{\alpha\beta}(\vec{q}) & -W_{\alpha\beta}+S_{\alpha\beta}(0)-\epsilon D_{\alpha\beta}(\vec{0}) \end{pmatrix},$$

where

$$W_{\alpha\beta}=\frac{1}{M}\sum_{\rho\neq 0}\left(\frac{\delta_{\alpha\beta}}{\rho}\frac{\partial U(\rho)}{\partial\rho}+\frac{x_{\alpha}x_{\beta}}{\rho}\frac{\partial}{\partial\rho}\frac{1}{\rho}\frac{\partial U(\rho)}{\partial\rho}\right)$$
$$\times[1-\exp(i\vec{q}\cdot\vec{\rho})], \quad (11)$$

$S_{\alpha\beta}(\vec{q})=C_{\alpha\beta}(\vec{q},d)$, $D_{\alpha\beta}(\vec{q})=C_{\alpha\beta}(\vec{q},d_i)$, and

$$C_{\alpha\beta}(\vec{q},z)=\frac{1}{M}\sum_{\vec{\rho}}\left(\frac{\delta_{\alpha\beta}}{\rho}\frac{\partial U(\sqrt{\rho^2+z^2})}{\partial\rho}\right.$$
$$\left.+\frac{x_{\alpha}x_{\beta}}{\rho}\frac{\partial}{\partial\rho}\frac{1}{\rho}\frac{\partial U(\sqrt{\rho^2+z^2})}{\partial\rho}\right)\exp(i\vec{q}\cdot\vec{\rho}),$$
$$(12)$$

with summations over the translation vectors $\vec{\rho}$ of the lattice. $S_{\alpha\beta}$ describes the (repulsive) interaction between the two particle layers seperated by a vertical distance d and $D_{\alpha\beta}$ the (attractive) interaction between the lower layer and the layer of the positive point charges with a vertical distance d_i.

Note that for our open system the dynamical matrix (10) is not Hermitian and its eigenvalues are generally complex. The matrix $W_{\alpha\beta}$ describes the behavior of a layered system, in which the two layers are noncoupled. A technique for calculating $W_{\alpha\beta}$ and its eigenvalues for the two-dimensional

Wigner crystal with a Coulomb interaction between particulates is given in Ref. [25]. For the calculation of the matrix $C_{\alpha\beta}$ for Debye-Hückel potentials Eq. (12) can be used directly. But for Coulomb potentials this sum converges very slowly. Therefore, the Fourier transform of Eq. (12) with fast convergence is taken

$$C_{\alpha\beta}(\vec{q},z)=\frac{2\pi e^2 Z^2}{MS}\sum_{\vec{g}}\frac{(g_{\alpha}+q_{\alpha})(g_{\beta}+q_{\beta})}{|\vec{g}+\vec{q}|}$$
$$\times\exp(-2\pi|\vec{g}+\vec{q}|z), \quad (13)$$

where the summation is performed over all translation vectors $\vec{g}$ of the reciprocal lattice.

Note that finding the spectrum of the matrix (10) allows us to treat the behavior of all eigenmodes of the dust crystal. Since it is the aim of this study to investigate the instability mechanism of the dust crystal, we restrict the problem to finding only those eigenvalues and eigenvectors of the dynamical matrix that have the maximum value of the real part $\mathrm{Re}(\lambda)$. The eigenvalues λ of the system (6) are given by the relation

$$\lambda_m^{1,2}=\frac{-\nu\pm\sqrt{\nu^2+4\eta_m}}{2}, \quad (14)$$

where η_m, $m=1,\ldots,4$, are the eigenvalues of the dynamical matrix A. The analysis of Eq. (14) allows us to obtain some general statements about the influence of friction on the crystal stability. Depending on η there are three possible types of solutions. For $\mathrm{Re}(\eta)>0$ the aligned situation is absolutely unstable for any values of the friction constant. For $\mathrm{Re}(\eta)<0$ the imaginary part $\mathrm{Im}(\eta)$ of the eigenvalue becomes important. For $\mathrm{Im}(\eta)=0$ the alignment is always stable. For $\mathrm{Im}(\eta)\neq 0$ there is a critical value of friction $\nu_{\star}$, above which the system is aligned and below which the system will be oscillatory unstable, i.e., it shows oscillations about the aligned positions with growing amplitude. In contrast, for a Hamiltonian system the eigenvalues of the dynamical matrix are always real, so the system is either stable or absolutely unstable independent of friction. The value $\nu_{\star}$ and corresponding oscillation frequency $\omega_{\star}$ are easily derived from relation (14)

$$\nu_{\star}=\mathrm{Im}(\eta)/\omega_{\star},\omega_{\star}=\sqrt{-\mathrm{Re}(\eta)}. \quad (15)$$

The eigenvalues η of the dynamic matrix A are obtained numerically. We normalize distances to the interparticle distance a and the time to the plasma frequency of the Wigner crystal $\omega_{pc}=\sqrt{4\pi e^2 Z^2/Ma^3}$. Then the system characteristics can be analyzed with the unitless parameters ν/ω_{pc}, ϵ, d/a, d_i/a, and r_d/a. Following the experimental results [11,13], the interlayer distance is set to $d/a=0.8$.

The critical value of the damping constant $\nu_{\star}$ and the frequency $\omega_{\star}$ as functions of the amplitude q of the wave vector $\vec{q}$ are shown in Fig. 7 for different orientations. It is well known [25] that only the values of the wave vector lying inside the irreducible element of the two-dimensional first Brillouin zone (see inset in Fig. 7) need to be considered. The most unstable mode (i.e., the one with the highest $\nu_{\star}$) is seen to be orientated in direction 3. This corresponds
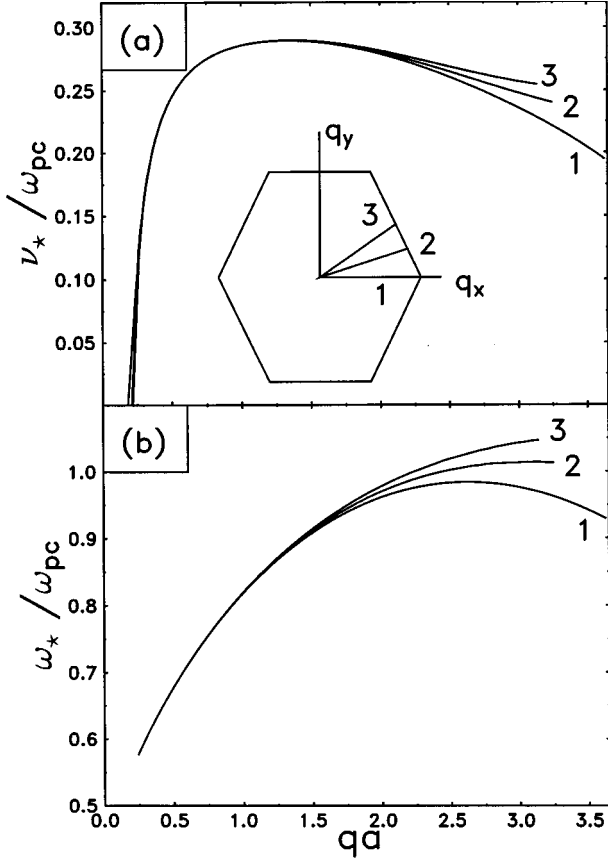
FIG. 7. Critical value of the (a) friction constant $\nu_\star$ and (b) corresponding oscillation frequency $\omega_\star$ versus the amplitude of the wave vector for different orientations. In the inset the first Brillouin zone for the two-dimensional hexagonal lattice is shown and the orientations of the wave vector are indicated. The reduced effective ion cloud charge is $\epsilon = 0.5$ and the distance is $d_i = 0.4a$.

to the direction connecting two neighboring particles in the direct hexagonal lattice. The increment $\gamma = \mathrm{Re}(\lambda)$ of the instability as a function of wavelength is given in Fig. 8 for different values of the friction constant. For small deviations of the friction constant $\delta\nu$ from its critical value, the eigenvalue has the form

$$\lambda = i\omega_\star - \frac{i\omega_\star}{\nu_\star + i\omega_\star}\delta\nu.$$

That means that near the critical friction the frequency $\mathrm{Im}(\lambda)$ weakly depends on the friction [see Fig. 12(a) for comparison with experiment] and $\mathrm{Re}(\lambda) \propto -\delta\nu$. Thus the increment of the instability $\mathrm{Re}(\lambda)$ increases linearly when the gas pressure is reduced below the critical value since the friction constant is proportional to the gas pressure [21].

B. Results for a definite orientation of the wave vector

From Fig. 7 it is seen that the critical friction $\nu_\star$ and frequency $\omega_\star$ only very weakly depend on the orientation of the wave vector. This is found to be true for a wide range of parameters. Therefore we treat the particular case $\vec{q} = (q,0)$ (curve 1 in Fig. 7) in more detail. For this specific wave
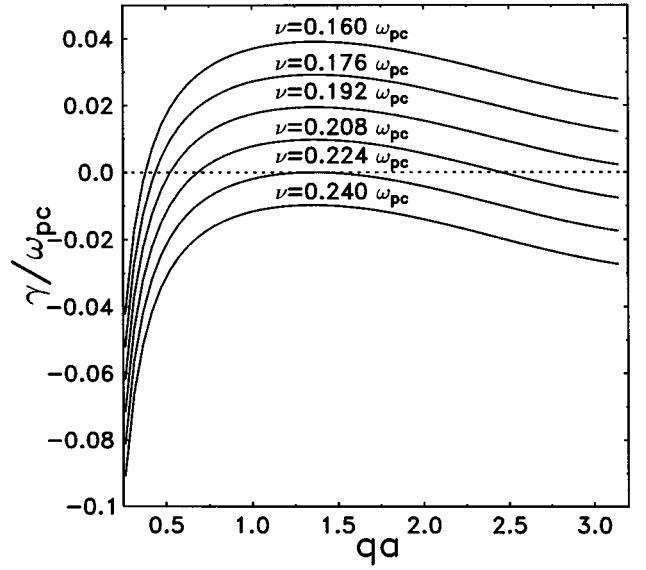
FIG. 8. Increment of the instability as a function of the amplitude of the wave vector of orientation 3 (inset of Fig. 7) for different values of the friction. Other parameters are the same as for Fig. 7.

vector the nondiagonal elements $W_{\alpha \neq \beta}$, $S_{\alpha \neq \beta}$, and $D_{\alpha \neq \beta}$ vanish and the eigenvalues η can be obtained analytically

$$\eta^\alpha_{1,2} = -W_{\alpha\alpha} + S_{\alpha\alpha}(0) - \frac{\epsilon}{2}D_{\alpha\alpha}(0)$$
$$\pm \sqrt{\left(\frac{\epsilon}{2}D_{\alpha\alpha}(0)\right)^2 - S_{\alpha\alpha}(q)[\epsilon D_{\alpha\alpha}(q) - S_{\alpha\alpha}(q)]}.$$
$$(16)$$

The two transverse modes $x_\alpha = x$ and $x_\alpha = y$ modes are decoupled. It should be emphasized that for $q = 0$ the eigenvalues $\eta^\alpha_{1,2}$ are real and the crystal structure may be either stable or absolutely unstable. Unstable oscillations appear for finite values of the wavelength. It can be shown that waves in the x direction become unstable first.

To investigate the conditions for alignment the term $\epsilon D_{xx}(0)$ has to be analyzed. This term is the first derivative of the restoring force F_x in the x direction. When the particulates of the two layers move relative to each other as a whole ($q = 0$), the eigenvalue $\eta = 2S_{\alpha\alpha}(0) - \epsilon D_{\alpha\alpha}(0)$ remains negative for

$$\epsilon > 2S_{\alpha\alpha}(0)/D_{\alpha\alpha}(0). \tag{17}$$

Note that the restoring force on the lower particulates outweighs the repulsion for the weaker condition $\epsilon > S_{\alpha\alpha}(0)/D_{\alpha\alpha}(0)$. This means that vertical alignment exists only when the radial attraction due to the positive ion clouds is at least twice as large as the repulsion between the negatively charged particulates. Otherwise the alignment will be unstable for any value of friction and a transition to a close-packed lattice takes place. If condition (17) is fulfilled, then

$$\omega_0 = \sqrt{\epsilon D_{\alpha\alpha}(0) - 2S_{\alpha\alpha}(0)}, \tag{18}$$
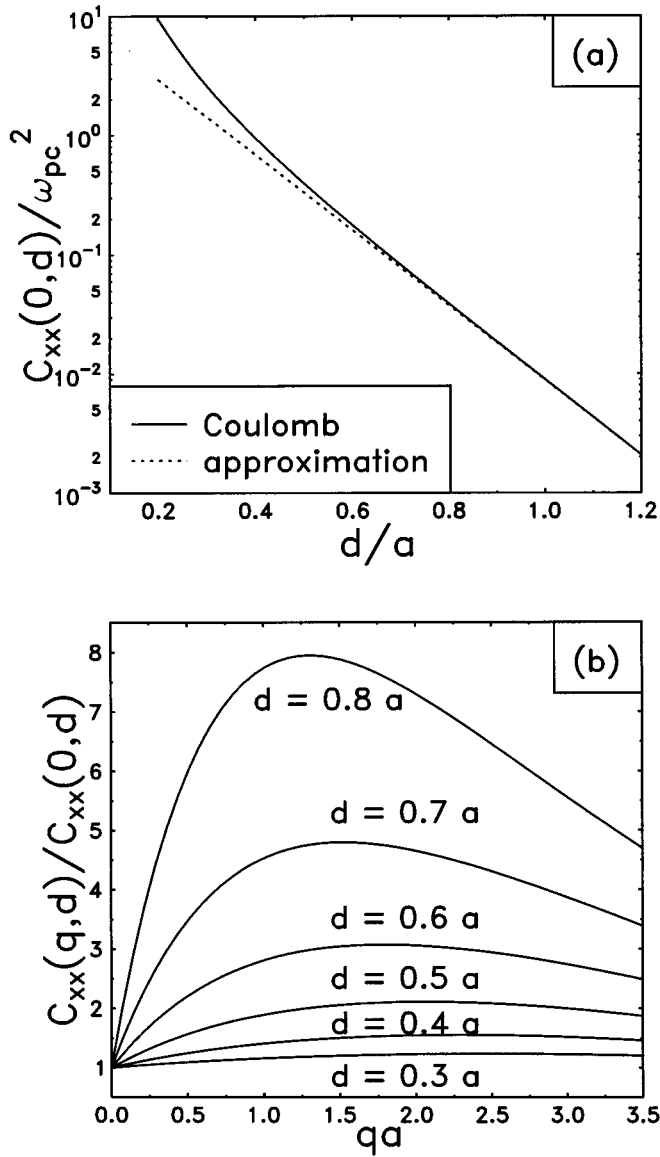
FIG. 9. (a) Coefficients $C_{xx}(0,d)$ as a function of distance for the Coulomb interaction (solid line). The dashed curve corresponds to the analytical approximation. (b) Ratio $C_{xx}(q,d)/C_{xx}(0,d)$ as a function of the amplitude of the wave vector directed along the x axis (line 1, inset of Fig. 7) for the different distances between ion clouds and the lower layer.

where ω_0 is the frequency of damped oscillations of the layers relative to each other. From the Monte Carlo results (Fig. 6), one can see that the ion-particulate restoring force is much larger than the repulsive force from upper particulates and $\epsilon D_{\alpha\alpha}(0) \gg S_{\alpha\alpha}(0)$. Consequently, the vertical alignment is stable and for a crude estimation of the damped frequency ω_0 one can use the first derivative of the restoring force. Since under this condition $\omega_0^2 \propto \epsilon$, in further discussions the dependence on the frequency ω_0 rather than on the reduced ion-cloud charge ϵ is used to describe the particulate-ion interaction. The dependence of the frequency ω_0 on the distance between the ion cloud and the lower particulates can be obtained on the basis of results given in Fig. 9. [Note that $C_{\alpha\alpha}(0,d) = S_{\alpha\alpha}(0)$ and $C_{\alpha\alpha}(0,d_i) = D_{\alpha\alpha}(0)$; see Eq. (12)].
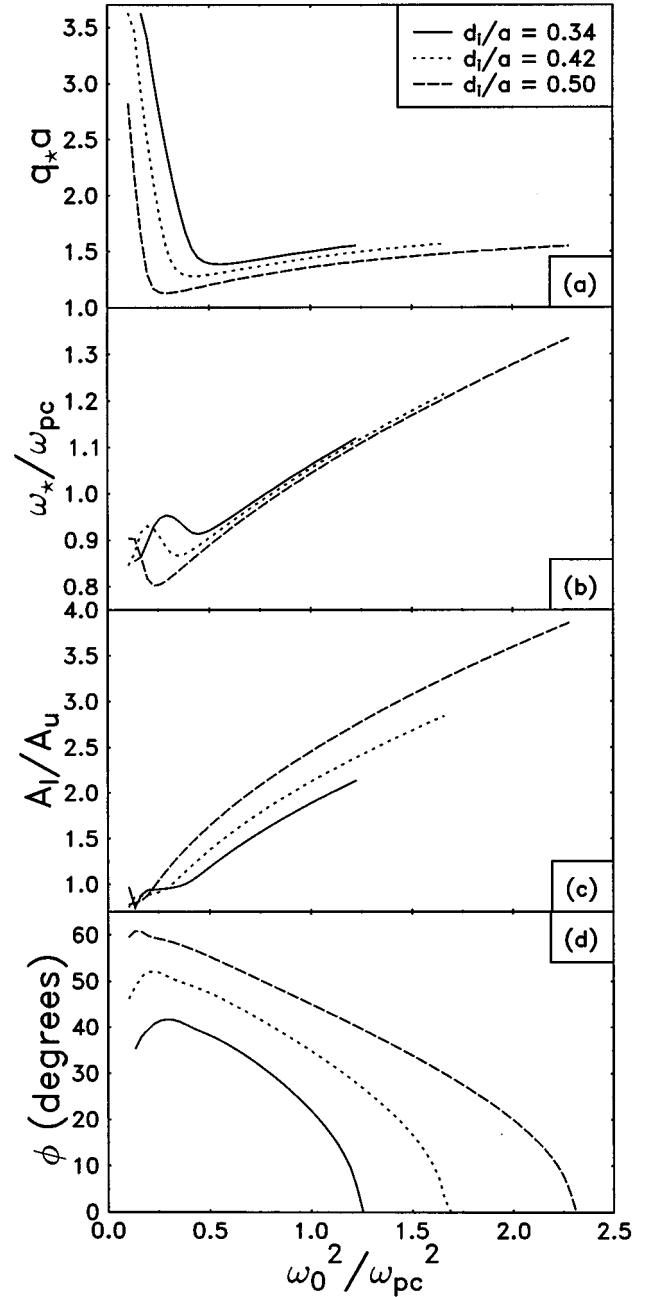
FIG. 10. (a) Amplitude of the wave vector corresponding to the most unstable situation, (b) associated frequencies, (c) ratio of oscillation amplitudes of the lower A_l and upper A_u particles, and (d) phase shift of the oscillation between the upper and the lower layer as a function of the characteristic frequency ω_0 for different d_i.

For a Coulomb potential and $2\pi z \gg a$ the first term in the sum (13) is sufficient to calculate $C_{\alpha\alpha}(0,z) \approx 4\pi\omega_{pc}^2 \exp(-4\pi z/\sqrt{3}a)$ [see the dashed curve in Fig. 9(a)]. The oscillation frequency of the layers relative to each other is proportional to the square root of the ion-cloud charge and decreases almost exponentially with the distance between the ion clouds and the lower layer.

For nonzero values of the wave vector, the instability of the dust crystal will occur with decreasing gas pressure if the expression under the square root in Eq. (16) is negative, i.e.,
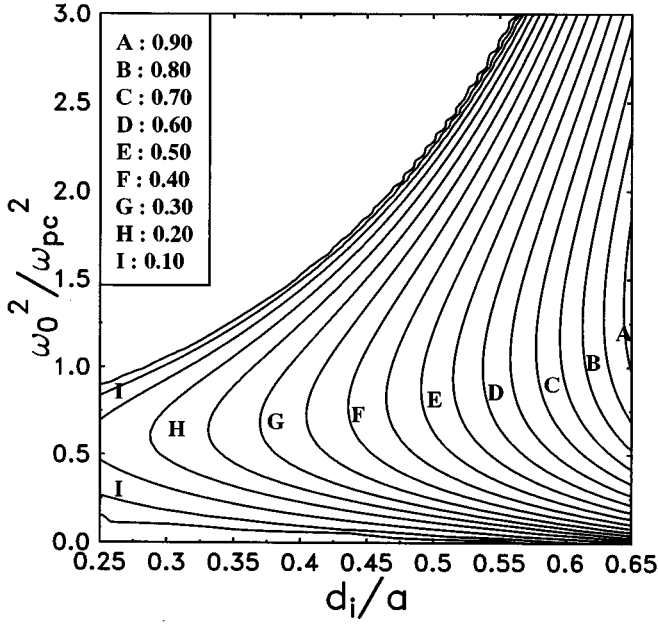
FIG. 11. Contour plot of the critical value of the friction constant in units of ω_{pc} over the characteristic frequency ω_0 and the distance d_i.

$$B = S_{\alpha\alpha}(q)[\epsilon D_{\alpha\alpha}(q) - S_{\alpha\alpha}(q)] - \left(\frac{\epsilon}{2} D_{\alpha\alpha}(0)\right)^2 > 0. \quad (19)$$

Setting $B = 0$, we obtain two critical values of the reduced charge of the ion cloud

$$\epsilon_{1,2} = \frac{S_{\alpha\alpha}(q)}{D_{\alpha\alpha}(0)}[D_{\alpha\alpha}(q) \pm \sqrt{D_{\alpha\alpha}(q)^2 - D_{\alpha\alpha}(0)^2}]. \quad (20)$$

For $\epsilon < \epsilon_1$ and $\epsilon > \epsilon_2$, B is negative and the system will be stable for any value of friction. Thus the enhancement of the ion-particulate interaction can lead to a stabilization of the dust crystal. The critical values of friction and the corresponding (undamped) oscillation frequency are given by the relations

$$\nu_\star = \sqrt{B}/\omega_\star, \qquad \omega_\star = \sqrt{W_{\alpha\alpha} + \omega_0^2/2}. \quad (21)$$

One can see that the frequency of the unstable mode is higher than the frequency $\sqrt{W_{\alpha\alpha}}$ for the crystal with non-coupled layers.

Since there is some uncertainty in the effective ion charge ϵ and the distance d_i, which are calculated above on the basis of a non-self-consistent approach in the MC model, the influence of these parameters on the stability of a dust crystal is investigated here. Calculations in a wide range of d_i and ω_0 were performed. First, we determined the most unstable wave vector $q_\star$, i.e., the wave vector with the highest critical value of the friction constant $\nu_\star$ [see Fig. 10(a)]. Hereafter the oscillation frequency $\omega_\star$ according to Eq. (21) is found as a function of ω_0, d_i for the given value $q_\star$ [see Fig. 10(b)]. Except for small ω_0, d_i, the most unstable wave vector is $q_\star a \approx 1.5$ and depends only weakly on the parameters of the ion cloud. For these values of the wave vector the frequency of the crystal plasma wave $\omega_\star$ is almost independent of the
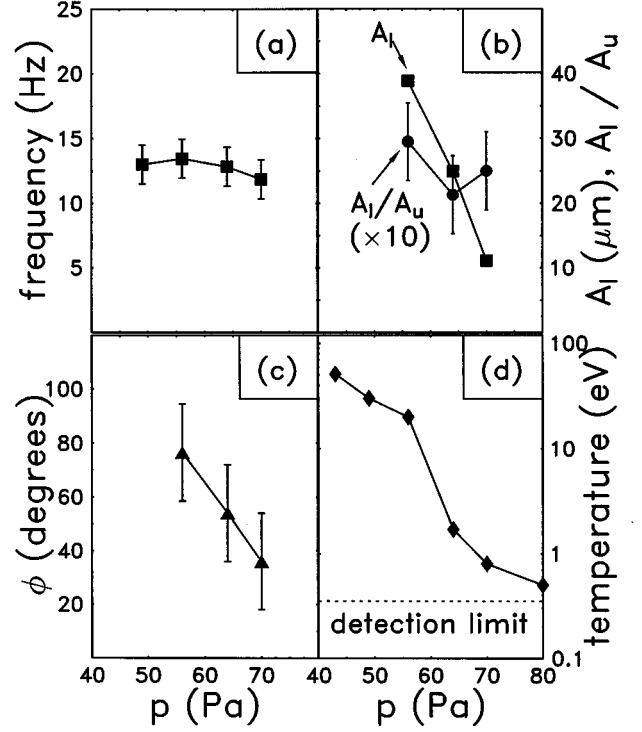
FIG. 12. Experimental values of the oscillation characteristics of the vertical aligned pairs as a function of gas pressure. (a) the frequency, (b) the amplitude of the lower particle A_l and the ratio of the amplitudes A_l/A_u, (c) the phase shift between the upper and the lower particle, and (d) the measured dust temperature.

wavelength. $\omega_\star$ lies in a range of $0.8\omega_{pc}-1.4\omega_{pc}$ and increases with ω_0 [see Fig. 10(b)]. Note that the system is most unstable for short wavelengths and hence the oscillations would be also expected for the liquid state, in which short-range order still exists. The most important characteristic of the instability is the critical value of friction $\nu_\star$, which is shown in Fig. 11. For a fixed distance between the ion cloud and the lower particulate $\nu_\star$ reaches its maximum value for a definite value of the charge of the ion cloud $\epsilon_\star$. Neglecting the dependence of $\omega_\star$ on ω_0 in the denominator of the relation (21), we estimate the value of $\epsilon_\star = 2S_{\alpha\alpha}(q)D_{\alpha\alpha}(q)/D_{\alpha\alpha}(0)^2$ from the condition of maximum of $\sqrt{B}$ [Eq. (19)]. Substituting this into Eq. (18), one obtains the value of the frequency

$$\omega_0^\star \approx \sqrt{S_{xx}(q_\star)D_{xx}(q_\star)/D_{xx}(0) - 2S_{xx}(0)},$$

for which the dust crystal is most unstable. Since the ratio of $D_{xx}(q_\star)/D_{xx}(0)$ increases with d_i [see Fig. 9(b)], both the value of $\omega_0^\star$ and the critical friction $\nu_\star$ increase with d_i.

C. Comparison with experiment

For the experimental conditions of the dust crystal the Monte Carlo calculations give the value $d_i/a = 0.35-0.5$ depending on gas pressure and particulate charge. At a gas pressure of about 100 Pa the reduced charge of an ion cloud is in the range $0.3n_t/\varrho - 0.4n_t/\varrho$. For typical values of

n_t/ϱ =1–3 the frequency ω_0 ranges from $0.7\omega_{pd}$ to $1.1\omega_{pc}$. The corresponding values of the critical friction are $\nu_\star = 0.25\omega_{pc} - 0.5\omega_{pc}$.

For experimental conditions the typical frequency ω_{pc} are predicted to be $\omega_{pc}/2\pi$ =10–20 Hz. Unstable oscillations develop with characteristic frequencies $\omega/2\pi$ = 7–22 Hz at critical friction in the range $2\pi \times (2.5-10)$ s^{-1} corresponding to a gas pressure of 30–150 Pa in helium [21]. From experimental data the critical value of friction is $2\pi \times 5$ s^{-1} (80 Pa) with a frequency of about 13 Hz [Fig. 12(a)], both within a range of the theoretical prediction. To carry out more precise estimations for the critical friction one has to use a self-consistent approach for ion motion simulation and more accurate experimental data for the dust particulate charge.

For further comparison of our model with the experimental results, the phase shift and the ratio between amplitudes of the particulate oscillation in the upper and lower layers is considered. For the simplest case $\vec{q} = (q,0)$, the ratio of the eigenvectors of perturbation is given by

$$\frac{\zeta_{x2}}{\zeta_{x1}} = \frac{\epsilon D_{\alpha\alpha}(0)/2 + i\sqrt{B}}{S_{\alpha\alpha}(q)}. \tag{22}$$

The ratio of the amplitudes of oscillation and the phase shift versus ω_0 for different distances between the ion cloud and lower layer are shown in Figs. 10(c) and 10(d), respectively. The oscillation amplitude of the lower particles is larger by a factor of 1.5–2.5 [experimentally 2–3, see Fig. 12(b)] than that of the upper particle. The absolute value of the oscillation amplitude increases with reduced pressure, finally leading to a dramatic increase in the dust temperature as one can see from Figs. 12(b) and 12(d). Since the imaginary part in Eq. (22) is less than its real part, the difference in the amplitudes increases almost linearly with ω_0^2, which is proportional to $\epsilon D_{\alpha\alpha}(0)$. Both the phase shift and the critical value of friction are proportional to $\sqrt{B}$. Therefore their behavior with changed system parameters has many features in common. In particular, they tend to zero for the same values of ω_0, d_i. For the experimental conditions $\omega_0 = 0.7\omega_{pc} - 1.1\omega_{pc}$ and $d_i = 0.35d - 0.5d$ the phase shift lies in the range 25°–50° [experimentally 30°–80°, Fig. 12(c)]

and increases with distance between the ion cloud and the lower layer, but decreases with the characteristic frequency ω_0.

The oscillations and the increase of dust temperature have also been observed for smaller particles in rf discharges in krypton by Thomas and Morfill [12]. The onset of instability occurs at a lower gas density. This can be understood since the friction exerted by krypton is larger than that of helium at the same pressure and the friction constant ν is larger for smaller particles.

VI. CONCLUSION

We have presented Monte Carlo calculations of the ion motion through a two-layer dust crystal located in the electrode sheath of a rf discharge in helium. The transverse deflection of ions by the electric field of the upper dust particles results in the formation of regions of enhanced ion space-charge density below the upper particles. The attractive forces of these ion clouds on the lower-layer particles are shown to lead to the vertical alignment as observed in many experiments. From these MC results an analytical model for the investigation of the stability of such an arrangement was derived. This model treats the many-body ion system as an effective pair potential resulting in a non-Hamiltonian system with nonreciprocal forces on lower and upper particles. The nonreciprocity is induced by the symmetry breaking of the ions streaming from above through the crystal. From the model the vertical alignment is found to become unstable, leading to oscillations of the aligned particles below a threshold value of friction. Furthermore, the characteristics of these unstable oscillations such as the wave frequency, the ratio between amplitudes of upper and lower particulates, and the phase shifts between the particle oscillations have been determined. These values are in close agreement with that found in experiments. So the melting transition is explained by the onset of self-excited oscillations due to a plasma-induced instability. The oscillations are the cause for the melting transition, not an effect of the phase transition.

[1] H. Ikezi, Phys. Fluids. **29**, 1764 (1986).

[2] J. H. Chu, J.-B. Du, and Lin I, J. Phys. D **27**, 296 (1994).

[3] J. H. Chu and Lin I, Physica A **205**, 183 (1994).

[4] J. H. Chu and Lin I, Phys. Rev. Lett. **72**, 4009 (1994).

[5] H. Thomas, G. E. Morfill, V. Demmel, J. Goree, B. Feuerbacher, and D. Möhlmann, Phys. Rev. Lett. **73**, 652 (1994).

[6] A. Melzer, T. Trottenberg, and A. Piel, Phys. Lett. A **191**, 301 (1994).

[7] T. Trottenberg, A. Melzer, and A. Piel, Plasma Sources Sci. Technol. **4**, 450 (1995).

[8] D. H. E. Dubin, Phys. Rev. Lett. **71**, 2753 (1993).

[9] V. A. Schweigert, M. I. Obrekht, Pis'ma Zh. Tekh. Fiz. **21**, 57 (1995) [Tech. Phys. Lett. **21**, 377 (1995)].

[10] M. O. Robbins, K. Kremer, and G. S. Grest, J. Chem. Phys. **88**, 3286 (1988).

[11] A. Melzer, A. Homann, and A. Piel, Phys. Rev. E **53**, 2757 (1996).

[12] H. Thomas and G. E. Morfill, Nature **379**, 806 (1996).

[13] A. Melzer, V. A. Schweigert, I. V. Schweigert, A. Homann, S. Peters, and A. Piel, Phys. Rev. E **54**, 46 (1996).

[14] M. D. Kilgore, J. E. Daugherty, R. K. Porteous, and D. B. Graves, J. Appl. Phys. **73**, 7195 (1993).

[15] J. Perrin, P. Molinas Mata, and P. Belenguer, J. Phys. D **27**, 2499 (1994).

[16] J. P. Boeuf, Phys. Rev. A **46**, 7910 (1992).

[17] J. E. Daugherty, M. D. Kilgore, R. K. Porteous, and D. B.

Graves, J. Appl. Phys.**72**, 3934 (1992).

[18] S. J. Choi and M. J. Kushner, J. Appl. Phys. **75**, 3351 (1994).

[19] F. Melands and J. Goree, Phys. Rev. E **52**, 5312 (1995).

[20] S. V. Vladimirov and M. Nambu, Phys. Rev. E **52**, 2172 (1995).

[21] P. S. Epstein, Phys. Rev. **23**, 710 (1924).

[22] P. P. Ewald, Ann. Phys. (Leipeig) **64**, 253 (1921).

[23] M. A. Lieberman and A. J. Lichtenberg, *Principles of Plasma Discharges and Materials Processing* (Wiley, New York, 1994).

[24] V. A. Schweigert, Pis'ma Zh. Tekh. Fiz. **21**, 69 (1995) [Tech. Phys. Lett. **21**, 476 (1995)]; in *Proceedings of the XXII International Conference on Phenomena in Ionized Gases*, edited by K. H. Becker, W. E. Carr, and E. E. Kunhardt (Stevens Institute of Technology, Hoboken, 1995).

[25] L. Bonsall and A. A. Maradudin, Phys. Rev. B **15**, 1959 (1977).